

Cite this: *Chem. Sci.*, 2024, **15**, 9733

All publication charges for this article have been paid for by the Royal Society of Chemistry

Received 30th April 2024
Accepted 15th May 2024

DOI: 10.1039/d4sc02850c

rsc.li/chemical-science

Boosting the degradation of antibiotics *via* peroxyomonosulfate activation with a Cu-based metal–organic framework[†]

Ying Wu,^a Gang Liang,^a Wen-Bin Li,^a Xiao-Feng Zhong,^a Yang-Yang Zhang,^a Jia-Wen Ye,^{ID}^a Tao Yang,^{*a} Zong-Wen Mo,^{ID}^{*a} and Xiao-Ming Chen,^{ID}^b

Highly efficient degradation of antibiotics is a huge challenge due to the extremely stable molecules and the potential for biological resistance. However, conventional degradation methods are limited to lower degradation rate, higher energy consumption and secondary pollution. Herein, we report a new Cu-based metal–organic framework (MOF), featuring classical planar trinuclear $[\text{Cu}_3(\mu_3\text{-O})]^{4+}$ clusters within the pores. The presence of the rich open metal sites and the large pore ratio, as well as the high catalytic activity of Cu^{2+} ions, are conducive to boosting the degradation of various antibiotics (>95%) under the activation of peroxyomonosulfate. Remarkably, this is the first MOF to achieve such exceptional catalytic performance under neutral and even alkaline conditions, which exceeds those of most reported materials. Mechanism investigation demonstrates that multiple active species were produced and promoted the degradation synergistically during the advanced oxidation processes.

Introduction

Antibiotics have been extensively used in the treatment of bacterial diseases, but most of them are non-metabolized and discharged into water directly, resulting in serious environmental pollution.¹ The traditional degradation methods (biological treatment and chlorination) are limited by the time-consuming processes and high-toxicity by-products. Therefore, highly effective methods are urgently needed for degrading the residual antibiotics.

As an emerging degradation technology, advanced oxidation processes (AOPs) based on the activation of persulfate (PS) or peroxyomonosulfate (PMS) with other technologies can produce highly reactive species (hydroxyl radicals (HO^\cdot), sulfate radicals ($\text{SO}_4^{\cdot-}$), singlet oxygen ($^1\text{O}_2$), superoxide radicals ($\text{O}_2^{\cdot-}$), etc.) for target degradation.^{2,3} Among them, $^1\text{O}_2$ and $\text{O}_2^{\cdot-}$, as the dominant reactive species, possess excellent resistance to the background components (inorganic ions, natural organic materials) of water, in contrast to the common radicals (HO^\cdot and $\text{SO}_4^{\cdot-}$). Furthermore, compared to the activation by UV light and heat, which is limited by the high energy consumption and complex

operation, heterogeneous catalytic activation possesses more outstanding activity by virtue of the multi-functionality (metal activation) and stability (avoiding secondary pollution from the materials).^{4–7} Therefore, the development of functional materials with high activity and stability, as well as being environmentally friendly, is still a huge challenge.⁸

Metal–Organic frameworks (MOFs) are well-known for the highly designable, tunable structures and pore surfaces, and have been applied in diverse fields,⁹ including catalytic oxidation.^{10–12} However, the application of pure MOFs for degrading antibiotics in AOPs is rarely reported, while the majority focus is on the degradation of dyes. For example, $[\text{Fe}_3\text{O}(\text{TBA})_3(\text{OH})(\text{H}_2\text{O})_2]$ (MIL-88A(Fe), $\text{H}_2\text{TBA} = \text{trans-2-butenedioic acid}$) and defective $[\text{Fe}_3\text{O}(\text{ATA})_3(\text{OH})(\text{H}_2\text{O})_2]$ (MIL-88B(NH_2)(Fe), $\text{H}_2\text{NBDC} = 2\text{-amino-1,4-benzene dicarboxylic acid}$) have been reported as catalysts, achieving more than 90% degradation of tetracycline (TC) and sulfamethoxazole (SMX) *via* activating the oxidants, demonstrating that the open metal sites (OMSs) are more conducive to the activation of PMS.^{13,14} Nevertheless, the high dosage of catalysts and the extra energy requirements, as well as the narrow pH range, significantly limit the application. On the other hand, the pores within MOFs usually act as confined space to load other functional molecules or metal nanoparticles to obtain composites, which can be used in the activation of PMS. For example, composite materials of $\text{Fe}@\text{C}$ and $\text{CoS}_x\text{--CuS}_x/\text{CF}$ derived from MOFs can degrade SMX with more than 95% degradation efficiencies.^{15,16} However, poor yield, high loss and limited OMSs for composite materials hinder the degradation performance.¹⁷ As far as we know, most of the literature reports on heterogeneous catalysts for

^aSchool of Environmental and Chemical Engineering, Jiangmen Key Laboratory of Synthetic Chemistry and Cleaner Production, Wuyi University, Jiangmen, Guangdong 529020, China. E-mail: wyuchemmwz@126.com; leoyanghit@126.com

^bMOE Key Laboratory of Bioinorganic and Synthetic Chemistry, GBRCE for Functional Molecular Engineering, School of Chemistry, IGCME, Sun Yat-Sen University, Guangzhou 510275, China

[†] Electronic supplementary information (ESI) available. CCDC 2309034. For ESI and crystallographic data in CIF or other electronic format see DOI: <https://doi.org/10.1039/d4sc02850c>



degradation of organics are focused on Fe-, Co-based catalysts. However, Cu^{2+} ions are more environment-friendly in comparison with Co^{2+} ions. On the other hand, the standard redox potential of $E_0(\text{Cu}^{2+}/\text{Cu}^+)$ (1.7 V) is much higher than that of $E_0(\text{Fe}^{3+}/\text{Fe}^{2+})$ (0.77 V), which is more favorable for the production of active species by activating PMS.¹⁸ Therefore, it is still a tremendous challenge to find functional MOFs that can achieve efficient degradation of antibiotics with high stability and numerous catalytically active sites.

Here, we synthesized a new MOF, $[\text{Cu}_3(\mu_3\text{-O})(\text{pypz})_3]\text{NO}_3$ guest, namely MAF-wyu2 (**1**, Hpypz = 4-(1H-pyrazol-4-yl)pyridine), which is a new member of metal-azolate frameworks (MAFs),¹⁹ and possesses rich OMSs based on the planar trinuclear $[\text{Cu}_3(\mu_3\text{-O})]^{4+}$ clusters. By virtue of the higher catalytic activity of Cu^{2+} ions and remarkable thermal and chemical stability, **1** can degrade common antibiotics (including SMX, oxytetracycline (OTC), sulfamethazine (SMZ), ciprofloxacin (CIP), TC) with high efficiency (95%+) within 30 minutes. In particular, the degradation performance for SMX, the most stable antibiotic, in AOPs reaches 100% based on PMS even in strong alkaline environments (pH = 11.0) with a low catalyst concentration (25 mg L⁻¹). **1** is the first MOF that can achieve such superior catalytic oxidation performance, and superior to most of the reported materials. The reactive oxygen species (ROS) quenching experiments and electron paramagnetic resonance (EPR) measurements verified the degradation mechanisms, suggesting that O_2^- and $^1\text{O}_2$ are the dominant active substances. Multi-cycle experiments and common ion interference tests proved that this MOF possesses good reusability and anion resistance.

Results and discussion

Solvochemical reaction of $\text{Cu}(\text{NO}_3)_2 \cdot 4\text{H}_2\text{O}$, Hpypz and 1H-1,2,4-triazole in *N,N*-dimethylacetamide (DMA) yielded the crystals of **1**. Single-crystal X-ray diffraction revealed that **1** crystallizes in the cubic space group $I\bar{4}3d$, containing one Cu^{2+} ion, one pypz⁻ ligand, one-third of $\mu_3\text{-O}$ and one-third of NO_3^- counter anion in an asymmetric unit (Fig. S1 and Table S1†). Three Cu^{2+} ions are bridged by the pyrazolate groups from three pypz⁻ ligands and $\mu_3\text{-O}$ into a classic planar trinuclear $[\text{Cu}_3(\mu_3\text{-O})]^{4+}$ cluster, exposing numerous OMSs within the pores (Fig. S2†). Each $[\text{Cu}_3(\mu_3\text{-O})]^{4+}$ cluster connects with the other six clusters through pypz⁻ ligands, obtaining an extended 3D framework (Fig. 1a and S4†). The counter NO_3^- anions are located near the trinuclear clusters in the pores. Regarding the planar trinuclear $[\text{Cu}_3(\mu_3\text{-O})(\text{Rpz})_3(\text{Rpy})_3]^+$ as 6-connected nodes and linear pypz⁻ as 2-connected linkers, the whole network forms a new 6-connected topology with the point symbol of {8⁶12⁹} {8}3 (Fig. S3†). Interestingly, there are 3D interconnected channels, with diameters of $8.6 \times 8.6 \text{ \AA}^2$ and $8.9 \times 11.7 \text{ \AA}^2$ along the *a*-axis, respectively (Fig. 1b and S4†). After ignoring the NO_3^- anions and solvate molecules, the pore ratio reaches 69.6% (Fig. 1b).

The powder X-ray diffraction (PXRD) pattern of as-synthesized **1** matches well with the simulated one, indicating the high purity and crystallinity (Fig. S5†). The scanning electron microscopy (SEM) image of **1** shows that there is a smooth

polyhedral morphology with a uniform particle size of about 25 μm (Fig. S6a and S6b†). Thermogravimetry analysis of **1** showed no obvious plateau, which can be attributed to the gradual removal of the high boiling point DMA molecules. After methanol (MeOH) exchange, **1** can be stable up to 200 °C (Fig. S7†). It is worth noting that **1** retained its framework after being immersed in aqueous solutions of pH range from 3.0 to 11.0 for six months, as well as in various organic solutions (*N,N*-diethylformamide (DEF), ethanol (EtOH), MeOH, acetonitrile (MeCN), diethyl ether (DEE)) for six months, indicating high chemical stability (Fig. S5†). It is worth noting that the PXRD patterns of the activated sample by various methods (direct heating activation, MeOH-exchanged activation and supercritical CO_2 (SC- CO_2) activation) were further obtained and indicated that the host-framework has been transformed into the amorphous state, probably owing to the large surface tension caused by the removal of guest molecules within the pores. Therefore, the N_2 adsorption isotherm of the host-framework cannot be measured. Interestingly, this amorphous state can be recovered to the as-synthesized phase after immersing in DMA, indicating that the structural transformations from the crystalline to the amorphous state are reversible (Fig. S8†).

Considering the excellent structural stability, and numerous OMSs within the framework,^{20–22} **1** may be a promising catalyst for efficient degradation of antibiotics by activating PMS. As far as we know, there are various types of antibiotics (*e.g.* tetracyclines, macrolides, quinolones, sulfonamides, *etc*), and sulfonamides (SAs, especially SMX) possess the most stability and poor biodegradability, leading to efficient degradation being extremely difficult. Therefore, degradation experiments were performed and showed that the degradation efficiency of SMX reached 100% within 20 min at pH = 7.0 by activating PMS (Fig. 2a and S9a†). In order to exclude the influence from the oxidation of PMS self-decomposition or the adsorption capacity of **1**, the solely PMS or **1** exhibits insignificant degradation (about 10%) and adsorption efficiency (about 20%), respectively (Fig. 2a and S9a†). Specifically, the adsorption rate of SMX to the host-framework is rapid owing to the coulombic interactions between the SMX⁻ and the cationic host-framework. However, the adsorption capacity of SMX is limited due to the large molecular size of SMX. In contrast, the catalytic performance boosted significantly with the addition of both **1** and PMS, achieving complete degradation within 20 min (k_{obs} increased to 0.389 min⁻¹). These results indicate that the OMSs within the host-framework can accelerate the activation of PMS and facilitate the degradation. At the same time, the morphology, particle size and PXRD patterns of **1** are maintained after degradation, except that the crystal surface was slightly rough and the cracks increased (Fig. S6c and S6d†).

Since the reaction parameters (such as pH, catalyst and oxidant concentrations) play crucial roles in the production of ROS, different experiments were performed to explore the degradation efficiency in PMS-based AOPs.²³ Initially, the effect of catalyst concentrations shows that the degradation efficiencies are positively correlated with the catalyst concentrations due to the increasing OMSs, which is conducive to producing more ROS by activating PMS.²⁴ Notably, the degradation



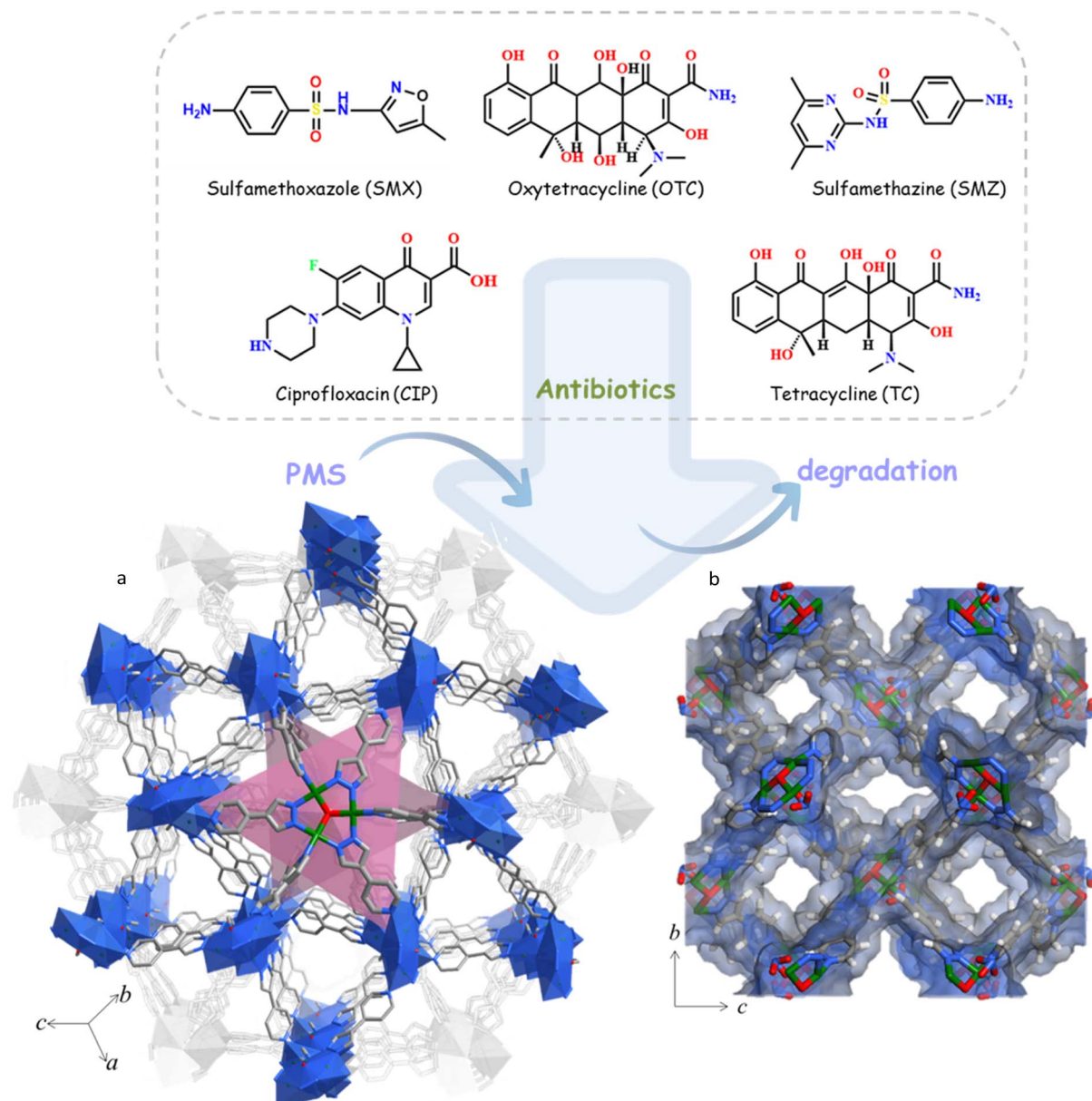


Fig. 1 (a) 3D coordination framework and (b) pore surface structure of **1**.

efficiency reached 100% within 30 min with the catalyst increased to 25 mg L^{-1} (Fig. 2b), corresponding to the k_{obs} value of 0.282 min^{-1} (Fig. S9b†). However, the degradation efficiency slightly decreases to 99% as the concentration increases to 50 mg L^{-1} , which is attributed to the quenching effect resulting from the reduction of ROS by the higher catalyst concentration.²⁵ These results indicate that the optimum catalyst concentration of 25 mg L^{-1} not only can avoid agglomeration effectively, but also produce sufficient ROS.

Besides, considering the different pH of various wastewaters and the stability of **1**, the SMX degradation in various pH shows that **1** possesses excellent degradation performance under a wide pH range from 5.0 to 11.0.²⁶ Specifically, the degradation efficiency of SMX reaches 98% at pH = 7.0. Considering SMX as a kind of dibasic acid (corresponding to $\text{pK}_{\text{a}1} = 1.7$ and $\text{pK}_{\text{a}2} =$

5.7), there are various forms of SMX with the pH changes according to the literature. The anionic form (SMX^-) prevails at $\text{pH} > 5.7$ and exhibits optimal reaction activity owing to the activation of the aniline portion within SMX, which is more susceptible to electrophilic attacks by PMS.²⁷ In other words, the excellent catalytic performances of **1** under neutral and alkaline conditions are attributed to the fact that the anionic SMX^- is not only more susceptible to attack by PMS by virtue of the coulombic interactions, but also adsorption to the cationic host-framework. The degradation efficiencies increase from 72% (0.057 min^{-1}) to 98% (0.154 min^{-1}) within the pH various from 5.0 to 9.0 (Fig. 2c and S9c†). Therefore, the synergistic interactions between SMX^- , the host-framework and ROS (generated by PMS activated with **1**) facilitate the degradation. At the same time, PMS is inclined to produce more ROS

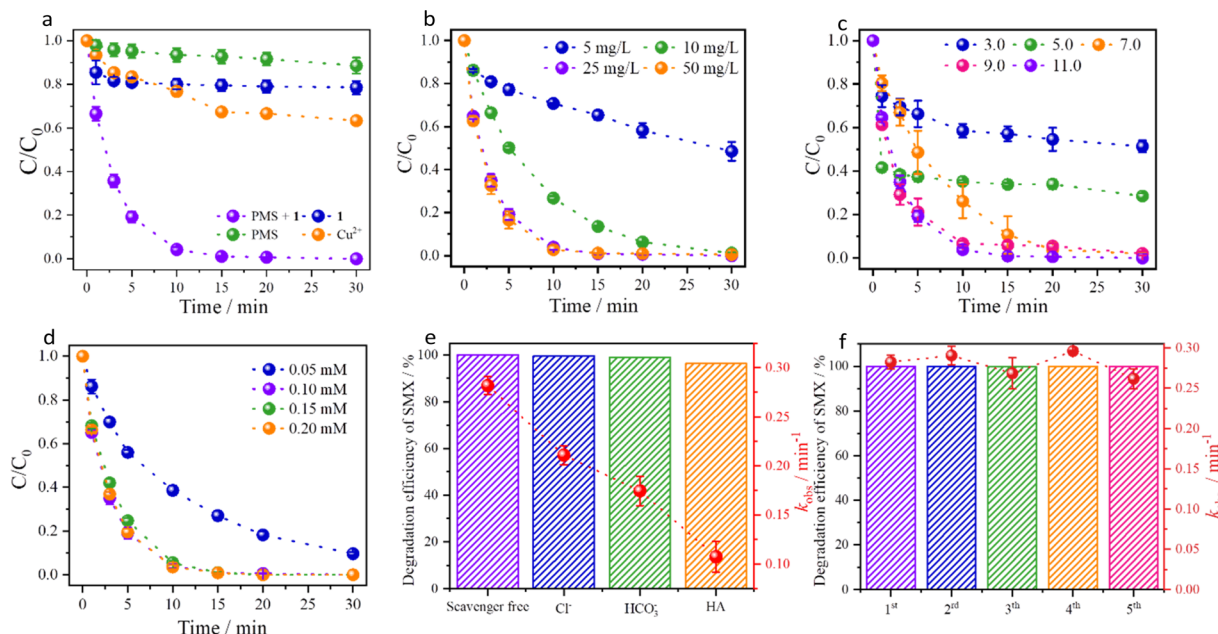


Fig. 2 (a) Comparison of the degradation performance in adsorption and/or catalysis. The influence of (b) catalyst concentrations, (c) pH, and (d) oxidant concentrations on the degradation of SMX. (e) The effect of the presence of common ions/molecules (1.0 mmol L^{-1}) on the degradation. (f) Recycling stability experiment for 5 times. (Experimental conditions: pH = 11.0, SMX = 5 μM , Catalyst = 25 mg L^{-1} , PMS = 100 μM , $T = 25^\circ\text{C}$.)

(e.g. $^1\text{O}_2$, O_2^\cdot) to accelerate the degradation under alkaline condition and the degradation efficiency reaches 100% (0.282 min^{-1}) at pH = 11.0. To the best of our knowledge, there are rare materials with excellent catalytic performance in such a wide pH range, and most of them work under neutral/weak alkaline conditions (Table S2†). In other words, **1** is the first MOF that can degrade SMX efficiently at pH = 11.0.

Additionally, the effect of oxidant concentrations (ranging from 0.05 mM to 0.20 mM) shows that the k_{obs} values are significantly correlated with the oxidant concentrations (providing more ROS), corresponding to that the oxidant concentrations increase from 0.083 min^{-1} at 0.05 mM to 0.321 min^{-1} at 0.20 mM (Fig. S9d†). It's worth noting that the k_{obs} increased slightly with the concentrations increasing from 0.10 mM to 0.20 mM, due to the presence of conversion and scavenging of highly oxidative ROS.^{25,28} Therefore, the optimum oxidant concentration can be determined as 0.10 mM (Fig. 2d).

It was reported that the activation of PMS in AOPs can produce various active species for degradation.²⁹⁻³¹ To determine the dominant active species under the optimal degradation conditions (25 mg L^{-1} **1**, 0.10 mM PMS and pH = 11.0), MeOH, L-ascorbic acid (AA) and furfuryl alcohol (FFA) can be employed as quenchers of hydroxyl radicals (HO^\cdot), sulfate radicals (SO_4^\cdot), superoxide radicals (O_2^\cdot) and singlet oxygen ($^1\text{O}_2$), respectively.³² It is clear that the degradation rates were slightly reduced (from 0.282 min^{-1} to 0.196 min^{-1}), whereas the efficiency (>97%) exhibits insignificant change in the presence of 10 mM MeOH, indicating that neither SO_4^\cdot nor HO^\cdot are dominant active species (Fig. 3a and S10†). In contrast, the degradation efficiencies and k_{obs} values are closely related to the quenching agents of AA and FFA, corresponding to 10%

(0.003 min^{-1}) and 19% (0.008 min^{-1}) at 10 mM AA/FFA (Fig. 3a, S11 and S12†). Obviously, the non-radical pathway of O_2^\cdot and $^1\text{O}_2$ plays key roles in the degradation process. Alternatively, the presence of the active species (SO_4^\cdot , HO^\cdot , O_2^\cdot and $^1\text{O}_2$) can be further confirmed by EPR measurements by using the spin traps of 5,5-dimethyl-1-pyrroline N-oxide (DMPO) and 2,2,6,6-tetramethyl-4-piperidinol (TEMP).³³ It is noted that no radical signal was observed with the addition of individual DMPO or PMS, while the typical adduct signals of DMPO- HO^\cdot , DMPO- SO_4^\cdot , as well as the typical sextuple signal of O_2^\cdot were detected in the presence of **1** and PMS,³⁴ which indicate that HO^\cdot , SO_4^\cdot and O_2^\cdot are produced in the AOPs (Fig. 3b and c). Moreover, there is a stronger triple signal of TEMP- $^1\text{O}_2$ after adding TEMP (Fig. 3d).³⁵ These results are consistent with the quenching experiments, demonstrating that the $^1\text{O}_2$ and O_2^\cdot play dominant roles in degrading SMX.

In order to investigate the recycling performance of **1**, multiple cycle tests were performed and showed that the degradation efficiencies remain above 95%, indicating the significant reusability and stability (Fig. 2f). To ensure the stability of the MOF during the degradation and eliminate the possibility of Cu^{2+} leaching, ICP measurement of Cu^{2+} ion leaching concentration after degradation was performed, and there was only 0.76 mg L^{-1} , which is lower than the value specified in the standard (<1.0 mg L^{-1} based on GB 25467-2010 or < 2.0 mg L^{-1} based on the European Union standard).¹⁶ In addition, a comparison experiment at 0.8 mg L^{-1} Cu^{2+} ion concentration (based on $\text{Cu}(\text{NO}_3)_2$) was also conducted and showed limited catalytic efficiency (36.62%) and k_{obs} (0.019 min^{-1}) (Fig. 2a and S9a†). In addition, considering that the complex components in sewage affect the degradation

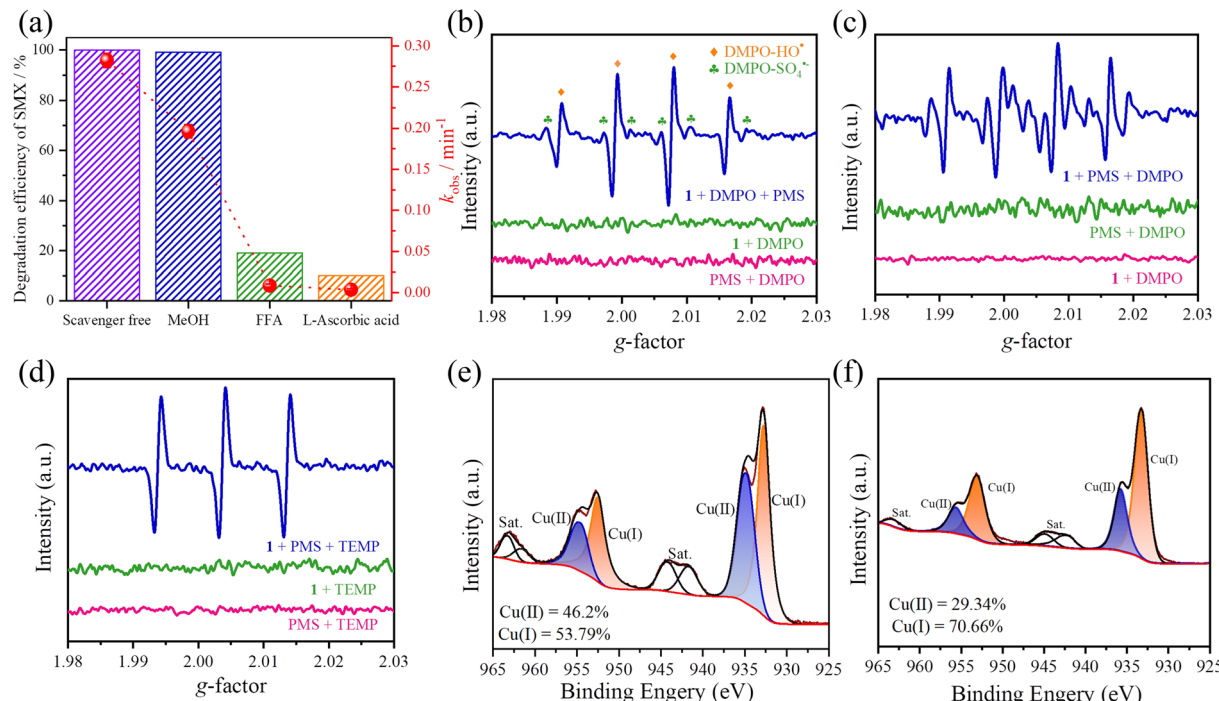


Fig. 3 (a) Effect of different scavengers on SMX degradation. (b) EPR spectra obtained with DMPO/HO $^{\cdot}$ and DMPO/SO $_{4}^{\cdot-}$, (c) DMPO/O $_{2}^{\cdot-}$ and (d) TEMP/O $_{2}^{\cdot-}$. High-resolution XPS spectra of Cu 2p (e) before and (f) after the degradation. (Experimental conditions: pH = 11.0, SMX = 5 $\mu\text{mol L}^{-1}$, Catalysts = 25 mg L^{-1} , PMS = 100 $\mu\text{mol L}^{-1}$, T = 25 °C, MeOH = 10 mmol L^{-1} , ascorbic acid = 10 mmol L^{-1} , FFA = 10 mmol L^{-1} .)

performance, degradation experiments in the presence of common ions (e.g., chloride ions (Cl $^-$), bicarbonate ions (HCO $_{3}^-$))/molecules showed insignificant effects on the degradation efficiency, except for humic acid (HA) (Fig. 2e, S13 and S14†). Interestingly, the degradation efficiencies and k_{obs} values decreased from 100% (0.282 min $^{-1}$) to 38% (0.017 min $^{-1}$) with the concentrations of HA increasing from 0 mg L^{-1} to 10 mg L^{-1} (Fig. S15†), owing to the functional groups in HA competing with SMX for ROS, as well as the blocking of HA on the OMSs of the material surface.^{39,40} These results show that the system exhibits great resistance to environmental anions in actual water and possesses strong degradation effects after filtering HA.

To further elucidate the relationship between ROS production and catalyst conductivity in the catalytic oxidation process, electrochemical and X-ray photoelectron spectroscopy (XPS) experiments were performed. First, the cyclic voltammetry curve of **1** exhibits strong reduction capacity, as well as electron transfer performance by virtue of the numerous OMSs and large specific surface area (Fig. S16a†). It is well known that the reaction rate of the material and electrode is related to the electron transfer resistance, corresponding to the smaller radius with lower impedance.⁴¹ Electrochemical impedance spectroscopy of **1** exhibits a smaller semicircular diameter, demonstrating the lower electron transfer impedance and higher charge transfer efficiency (Fig. S16b†). In addition, XPS results clearly show the presence of C, N, O and Cu in **1**, and the spectra of other elements were calibrated by the binding energies of C (284.8 eV). Specifically, the peaks at 932.3 eV, 952.2 eV

and 934.7 eV, 954.6 eV correspond to Cu(I) and Cu(II), respectively (Fig. 3e and f), illustrating the valence change of Cu in the degradation.⁴² It is noteworthy that the relative ratio of Cu(II) decreases from 46.2% to 29.3%, while that of Cu(I) increases from 53.8% to 70.7%, demonstrating that a portion of Cu(II) within the host-framework has been converted to Cu(I) in AOPs. These results indicated that there is a reduction process of Cu(II) to Cu(I) due to the transfer of the peaks in Cu 2p $_{1/2}$ and Cu 2p $_{3/2}$ towards the region of lower binding energy.

Based on the above results, the mechanism of degradation can be proposed as follows: PMS is activated by the Cu $^{2+}$ ions in **1**, facilitating the generation of ROS in the free radical and non-radical pathways and the transition of the metal valence state, as well as the formation of intermediates/products during the degradation (Fig. 4). First, for the free radical pathway, HSO $_{5}^-$ (PMS) ions are decomposed into SO $_{5}^{2-}$ ions at pH > 9.4 (eqn (1)), generating O $_{2}^{\cdot-}$ species in the aqueous solution simultaneously (eqn (2)). Furthermore, the Cu $^{2+}$ ions as the intermediate mediators obtain electrons from PMS more efficiently, triggering the decomposition of HSO $_{5}^-$ and generation of O $_{2}^{\cdot-}$ and SO $_{5}^{\cdot-}$ (eqn (3) and (4)). Simultaneously, the Cu $^{+}$ ions react with HSO $_{5}^-$, producing HO $^{\cdot}$ and SO $_{4}^{\cdot-}$ (eqn (5) and (6)). It is worth noting that SO $_{4}^{\cdot-}$ are only available at pH < 10.0. Therefore, SO $_{4}^{\cdot-}$ are hydrolyzed to produce a large amount of HO $^{\cdot}$ under extremely alkaline conditions, which is conducive to the degradation (eqn (7)). On the other hand, in the non-radical pathway, the Cu $^{2+}$ ions can activate HSO $_{5}^-$ to form SO $_{5}^{\cdot-}$, and subsequently generate $^1\text{O}_2$ by recombination (eqn (8) and (9)). Consequently, SMX can be degraded to various products with lower toxicity than SMX in the

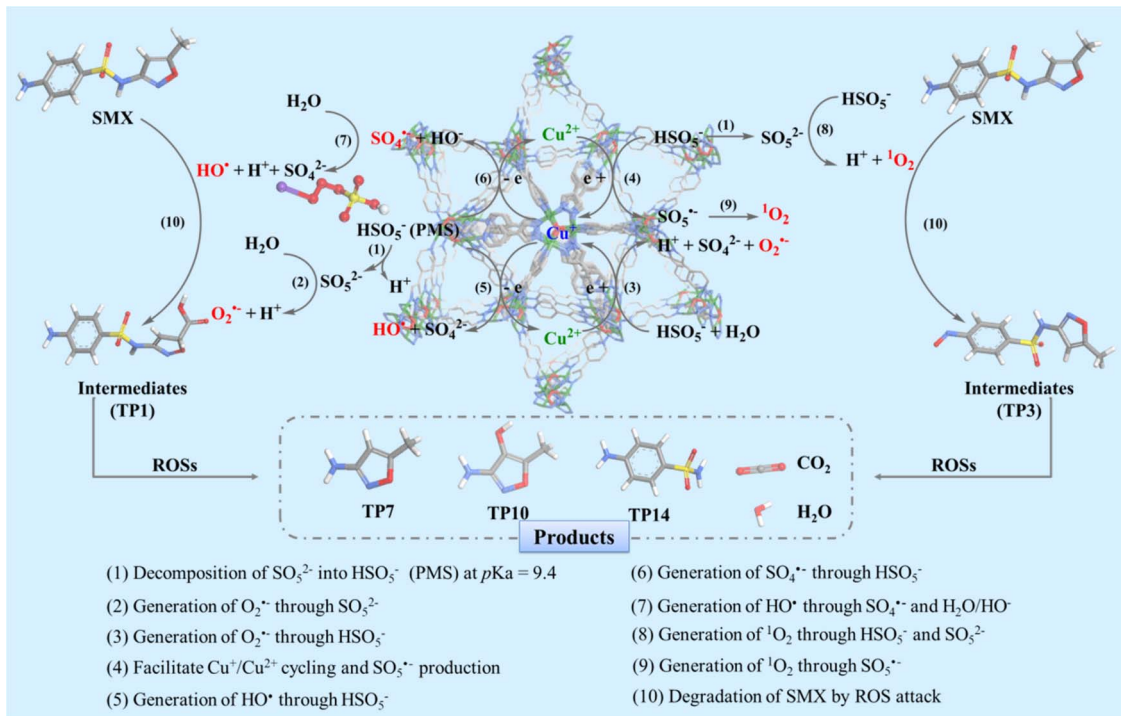


Fig. 4 The proposed mechanism of SMX degradation by PMS activation with 1.

presence of ROS (HO^{\cdot} , $\text{SO}_4^{\cdot-}$, $\text{O}_2^{\cdot-}$, ${}^1\text{O}_2$) (eqn (10)), and even to CO_2 and H_2O (Fig. 4 and S17†).

Since the application of pure MOFs for antibiotic degradation is rarely reported, various types of classical MOFs, such as $[\text{Fe}(\text{OH})(\text{BDC})]$ (MIL-53(Fe), H_2BDC = 1,4-benzene dicarboxylic acid), $[\text{Fe}_3(\mu_3-\text{O})\text{Cl}(\text{H}_2\text{O})_2(\text{BDC})_3]$ (MIL-101(Fe)), $[\text{Cu}_3(\mu-\text{OH})(\text{pzca})_3(\text{H}_3\text{O})]$ (H_2pzca = 1*H*-pyrazole-4-carboxylic acid), $[\text{Cu}_3(\text{BTC})_2(\text{H}_2\text{O})_3]$ (HKUST-1, H_3BTC = benzene-1,3,5-tricarboxylic acid), $[\text{Co}_2(\text{dhbdc})(\text{H}_2\text{O})_2]$ (MOF-74, H_4dhbdc =

2,5-dihydroxyterephthalic acid), $[(\text{Zn}_4\text{O})_3(\text{Cu}_3(\text{PyCA})_3)_4(\text{BDC})]$ (FDM-6, H_2PyC = 4-pyrazolecarboxylic acid), $[\text{Cu}_2\text{Zn}_3(\text{BTDD})_3\text{Cl}_4]$ (Cu-MFU-4*l*, H_2BTDD = bis[1*H*-1,2,3-triazolo[4,5-*b*],[4',5'-*i*]]dibenz[1,4]dioxin), and a coordination compound of $[\text{Cu}_3(\text{PyCA})_3]$ (HPyCA = 1*H*-pyrazole-4-carbaldehyde), were selected as catalysts to evaluate the SMX degradation performance under the same conditions to verify the effects of the types of OMSs or various metal ions for the degradation performance. Interestingly, both MIL-53 and MIL-101 containing the OMSs of Fe^{3+}

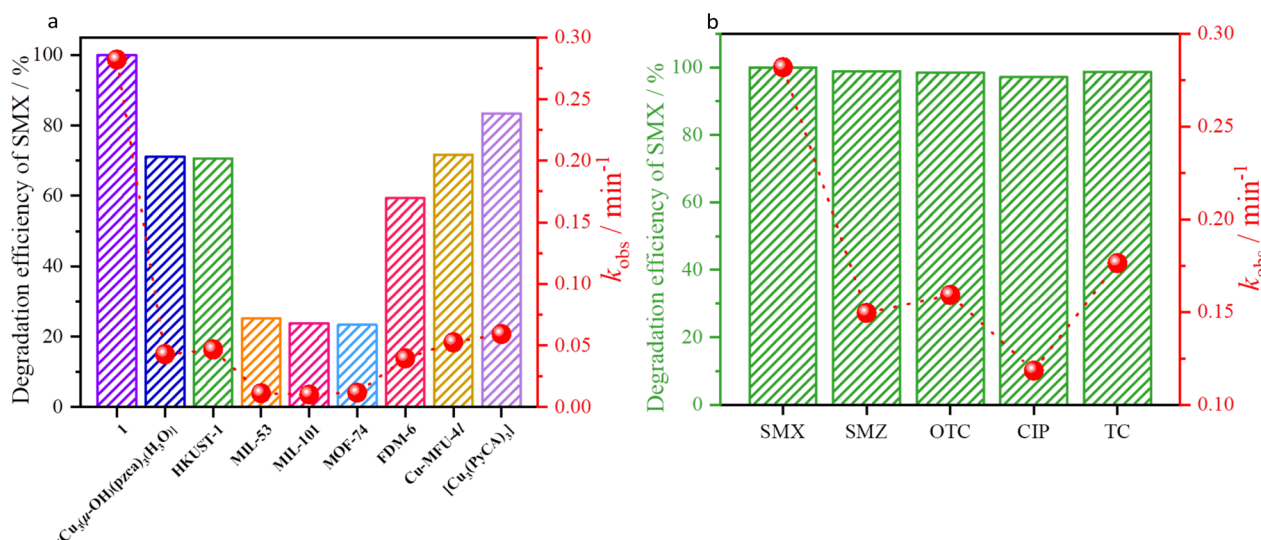


Fig. 5 (a) The SMX degradation performance based on various materials, and (b) the degradation of different antibiotics by PMS activated by 1. (Experimental conditions: $\text{pH} = 11.0$, antibiotics = $5 \mu\text{mol L}^{-1}$, catalysts = 25 mg L^{-1} , PMS = $100 \mu\text{mol L}^{-1}$, $T = 25^\circ\text{C}$.)

ions, and MOF-74 containing the OMSs of Co^{2+} ions, exhibit poor degradation efficiencies of less than 40%, while the degradation performance of HKUST-1 containing the OMSs of Cu^{2+} ions reaches 71% ($k_{\text{obs}} = 0.047 \text{ min}^{-1}$). Although the standard redox potential of $E_0(\text{Co}^{3+}/\text{Co}^{2+})$ (1.92 V) is much higher than $E_0(\text{Cu}^{2+}/\text{Cu}^+)$ (1.7 V) and $E_0(\text{Fe}^{3+}/\text{Fe}^{2+})$ (0.77 V), the larger pore ratio of **1** is more favorable for the diffusion of the antibiotics into the pores than other MOFs. These results imply that the degradation performance is not only related to the types of OMSs, but also to the porosity of the host-framework. To further demonstrate the role of planar trinuclear clusters, the degradation performance of $[\text{Cu}_3(\mu\text{-OH})(\text{pzca})_3(\text{H}_3\text{O})]$, FDM-6, Cu-MFU-4*l* and $[\text{Cu}_3(\text{PyCA})_3]$ containing similar planar trinuclear units showed that **1** possesses the most significant degradation efficiency and rate constant (100%, 0.282 min^{-1}) compared to $[\text{Cu}_3(\mu\text{-OH})(\text{pzca})_3(\text{H}_3\text{O})]$ (71%, 0.043 min^{-1}) $[\text{Cu}_3(\text{PyCA})_3]$ (83.4%, 0.059 min^{-1}), FDM-6 (59.3%, 0.039 min^{-1}) and Cu-MFU-4*l* (71.7%, 0.053 min^{-1}) (Fig. 5a and Table S3†), indicating that the significant degradation performance is the result of synergistic effect of the cationic host-framework and density of OMSs, as well as the porosity. At the same time, the Turnover Number (TON) and Turnover Frequency (TOF) were also calculated and indicated that the TOF and TON of **1** are 0.038 min^{-1} and 0.008 min^{-1} , respectively, which are superior to those of the selected materials (Table S3†).⁴³ In addition, the PXRD patterns of catalysts were retained after the degradation (Fig. S18†).

Considering that there are various antibiotics in the actual water, the degradation efficiencies of **1** towards OTC, SMZ, CIP, and TC were also tested. The results show that **1** can activate PMS to achieve high-efficiency degradation (>95% within 30 min) of other common antibiotics, demonstrating that **1** possesses excellent activity and adaptability for various organic contaminants (Fig. 5b).

Conclusions

In summary, a new Cu-based MOF with planar trinuclear $[\text{Cu}_3(\mu_3\text{-O})]^{4+}$ clusters was synthesized. By virtue of the combination of excellent stability, rich OMSs in the framework and high activity of Cu^{2+} ions, as well as the large pore ratio, this MOF can effectively activate peroxymonosulfate to degrade various antibiotics by producing highly active species. Remarkably, the degradation is applicable not only for lower catalyst concentrations (25 mg L^{-1}), but also in a wide pH range. In particular, the degradation rate can reach 0.282 min^{-1} at $\text{pH} = 11.0$. Mechanism studies demonstrate that the redox circulation between $\text{Cu}(\text{II})$ and $\text{Cu}(\text{I})$ promotes the participation of free and non-free radicals (including, HO^\cdot , SO_4^{2-} , O_2^{2-} , ${}^1\text{O}_2$) in the process of degradation, among which O_2^{2-} and ${}^1\text{O}_2$ are dominant. These results provide insights into designing potent catalysts with outstanding activity and long-term stability for degrading organic pollutants.

Data availability

All experimental supporting data are available in the ESI.†

Author contributions

Ying Wu: investigation, data curation, writing – original draft. Gang Liang: methodology, data curation, resources. Wen-Bin Li: methodology, data curation, resources. Xiao-Feng Zhong: resources, methodology. Yang-Yang Zhang: resources, methodology. Jia-Wen Ye: writing – review & editing. Tao Yang: writing – original draft, writing – review & editing, formal analysis. Zong-Wen Mo: project administration, funding acquisition, writing – original draft, writing – review & editing, formal analysis. Xiao-Ming Chen: supervision, project administration, funding acquisition.

Conflicts of interest

The authors declare no competing financial interest.

Acknowledgements

This work was supported by the NSFC (22101210), Municipal Science and Technology Bureau (Jiangke 2021-76), the Foundation of Department of Education of Guangdong Province (2023KTSCX152, 2022ZDJS027).

Notes and references

- 1 P. H. Wang, T. Zhou, R. Wang and T. T. Lim, Carbon-sensitized and nitrogen-doped TiO_2 for photocatalytic degradation of sulfanilamide under visible-light irradiation, *Water Res.*, 2011, **45**, 5015–5026.
- 2 Y. P. Bao, T. T. Lim, R. Wang, R. D. Webster and X. Hu, Urea-assisted one-step synthesis of cobalt ferrite impregnated ceramic membrane for sulfamethoxazole degradation via peroxymonosulfate activation, *Chem. Eng. J.*, 2018, **343**, 737–747.
- 3 J. L. Wang and S. Z. Wang, Reactive species in advanced oxidation processes: Formation, identification and reaction mechanism, *Chem. Eng. J.*, 2020, **401**, 126158.
- 4 Y. Feng, D. L. Wu, Y. Deng, T. Zhang and K. M. Shih, Sulfate Radical-Mediated Degradation of Sulfadiazine by CuFeO_2 Rhombohedral Crystal-Catalyzed Peroxymonosulfate: Synergistic Effects and Mechanisms, *Environ. Sci. Technol.*, 2016, **50**, 3119–3127.
- 5 J. L. Wang and S. Z. Wang, Activation of persulfate (PS) and peroxymonosulfate (PMS) and application for the degradation of emerging contaminants, *Chem. Eng. J.*, 2018, **334**, 1502–1517.
- 6 S. Z. Wang, H. Y. Liu and J. L. Wang, Nitrogen, sulfur and oxygen co-doped carbon-armored $\text{Co}/\text{Co}_9\text{S}_8$ rods ($\text{Co}/\text{Co}_9\text{S}_8@\text{N-S-O-C}$) as efficient activator of peroxymonosulfate for sulfamethoxazole degradation, *J. Hazard. Mater.*, 2020, **387**, 121669.
- 7 V. L. Pham, D. G. Kim and S. O. Ko, Oxidative degradation of the antibiotic oxytetracycline by $\text{Cu}@\text{Fe}_3\text{O}_4$ core-shell nanoparticles, *Sci. Total Environ.*, 2018, **631–632**, 608–618.
- 8 J. F. Yan, J. L. Peng, L. D. Lai, F. Z. Ji, Y. H. Zhang, B. Lai, Q. X. Chen, G. Yao, X. Chen and L. P. Song, Activation



CuFe_2O_4 by Hydroxylamine for Oxidation of Antibiotic Sulfamethoxazole, *Environ. Sci. Technol.*, 2018, **52**, 14302–14310.

9 A. Kirchon, L. Feng, H. F. Drake, E. A. Joseph and H. C. Zhou, From fundamentals to applications: a toolbox for robust and multifunctional MOF materials, *Chem. Soc. Rev.*, 2018, **47**, 8611–8638.

10 L. Jiao, Y. Wang, H. L. Jiang and Q. Xu, Metal-Organic Frameworks as Platforms for Catalytic Applications, *Adv. Mater.*, 2018, **30**, 23.

11 P. S. Murthy, L. Wilson, X. M. Zhang, W. B. Liang and J. Huang, Ni-doped metal-azolate framework-6 derived carbon as a highly active catalyst for CO_2 conversion through the CO_2 hydrogenation reaction, *Carbon Capture Sci. Technol.*, 2023, **7**, 10.

12 H. H. Hu, Z. Y. Wang, L. Y. Cao, L. Z. Zeng, C. K. Zhang, W. B. Lin and C. Wang, Metal-organic frameworks embedded in a liposome facilitate overall photocatalytic water splitting, *Nat. Chem.*, 2021, **13**, 11.

13 J. Sun, J. Q. Wan, Y. Wang, Z. C. Yan, Y. W. Ma, S. Ding, M. Tang and Y. C. Xie, Modulated construction of Fe-based MOF via formic acid modulator for enhanced degradation of sulfamethoxazole: Design, degradation pathways, and mechanism, *J. Hazard. Mater.*, 2022, **429**, 16.

14 Y. Zhang, J. B. Zhou, X. Chen, L. Wang and W. Q. Cai, Coupling of heterogeneous advanced oxidation processes and photocatalysis in efficient degradation of tetracycline hydrochloride by Fe-based MOFs: Synergistic effect and degradation pathway, *Chem. Eng. J.*, 2019, **369**, 745–757.

15 M. J. Pu, J. Q. Wan, F. Z. Zhang, M. L. Brusseau, D. Q. Ye and J. F. Niu, Insight into degradation mechanism of sulfamethoxazole by metal-organic framework derived novel magnetic $\text{Fe}@\text{C}$ composite activated persulfate, *J. Hazard. Mater.*, 2021, **414**, 125598.

16 A. F. Du, H. F. Fu, P. Wang, C. Zhao and C. C. Wang, Enhanced catalytic peroxymonosulfate activation for sulfonamide antibiotics degradation over the supported $\text{CoS}_x\text{-CuS}_x$ derived from ZIF-L (Co) immobilized on copper foam, *J. Hazard. Mater.*, 2022, **426**, 128134.

17 W. W. Zhang, Y. Su, X. M. Zhang, Y. Yang and X. H. Guo, Facile synthesis of porous NiCo_2O_4 nanoflakes as magnetic recoverable catalysts towards the efficient degradation of RhB, *RSC Adv.*, 2016, **6**, 64626–64633.

18 D. T. Oyekunle, E. A. Gendy, J. Ifthikar and Z. Q. Chen, Heterogeneous activation of persulfate by metal and non-metal catalyst for the degradation of sulfamethoxazole: A review, *Chem. Eng. J.*, 2022, **437**, 135277.

19 J. P. Zhang, Y. B. Zhang, J. B. Lin and X. M. Chen, Metal Azolate Frameworks: From Crystal Engineering to Functional Materials, *Chem. Rev.*, 2012, **112**, 1001–1033.

20 H. Z. Chi, Z. Y. Wang, X. He, J. Q. Zhang, D. Wang and J. Ma, Activation of peroxymonosulfate system by copper-based catalyst for degradation of naproxen: Mechanisms and pathways, *Chemosphere*, 2019, **228**, 54–64.

21 C. Alexopoulou, A. Petala, Z. Frontistis, C. Drivas, S. Kennou, D. I. Kondarides and D. Mantzavinos, Copper phosphide and persulfate salt: A novel catalytic system for the degradation of aqueous phase micro-contaminants, *Appl. Catal., B*, 2019, **244**, 178–187.

22 W. D. Oh, Z. L. Dong and T. T. Lim, Generation of sulfate radical through heterogeneous catalysis for organic contaminants removal: Current development, challenges and prospects, *Appl. Catal., B*, 2016, **194**, 169–201.

23 F. Wang, H. F. Fu, F. X. Wang, X. W. Zhang, P. Wang, C. Zhao and C. C. Wang, Enhanced catalytic sulfamethoxazole degradation via peroxymonosulfate activation over amorphous $\text{CoS}_x@\text{SiO}_2$ nanocages derived from ZIF-67, *J. Hazard. Mater.*, 2022, **423**, 126998.

24 A. Jawad, J. Lang, Z. W. Liao, A. Khan, J. Ifthikar, Z. N. Lv, S. J. Long, Z. L. Chen and Z. Q. Chen, Activation of persulfate by $\text{CuO}_x@\text{Co-LDH}$: A novel heterogeneous system for contaminant degradation with broad pH window and controlled leaching, *Chem. Eng. J.*, 2018, **335**, 548–559.

25 J. Y. Cao, L. D. Lai, B. Lai, G. Yao, X. Chen and L. P. Song, Degradation of tetracycline by peroxymonosulfate activated with zero-valent iron: Performance, intermediates, toxicity and mechanism, *Chem. Eng. J.*, 2019, **364**, 45–56.

26 X. H. Yi, H. D. Ji, C. C. Wang, Y. Li, Y. H. Li, C. Zhao, A. O. Wang, H. F. Fu, P. Wang, X. Zhao and W. Liu, Photocatalysis-activated SR-AOP over PDINH/MIL-88A(Fe) composites for boosted chloroquine phosphate degradation: Performance, mechanism, pathway and DFT calculations, *Appl. Catal., B*, 2021, **293**, 120229.

27 A. W. Wang, J. X. Ni, W. Wang, D. M. Liu, Q. Zhu, B. X. Xue, C. C. Chang, J. Ma and Y. Zhao, MOF Derived Co-Fe nitrogen doped graphite carbon@crosslinked magnetic chitosan Micro-nanoreactor for environmental applications: Synergy enhancement effect of adsorption-PMS activation, *Appl. Catal., B*, 2022, **319**, 121926.

28 Y. C. Du, W. J. Ma, P. X. Liu, B. H. Zou and J. Ma, Magnetic CoFe_2O_4 nanoparticles supported on titanate nanotubes ($\text{CoFe}_2\text{O}_4/\text{TNTs}$) as a novel heterogeneous catalyst for peroxymonosulfate activation and degradation of organic pollutants, *J. Hazard. Mater.*, 2016, **308**, 58–66.

29 G. P. Anipsitakis and D. D. Dionysiou, Radical generation by the interaction of transition metals with common oxidants, *Environ. Sci. Technol.*, 2004, **38**, 3705–3712.

30 Y. P. Bao, W. D. Oh, T. T. Lim, R. Wang, R. D. Webster and X. Hu, Elucidation of stoichiometric efficiency, radical generation and transformation pathway during catalytic oxidation of sulfamethoxazole via peroxymonosulfate activation, *Water Res.*, 2019, **151**, 64–74.

31 S. Y. Zhao, Y. K. Long, Y. P. Su, S. B. Wang, Z. T. Zhang and X. J. Zhang, Cobalt-Enhanced Mass Transfer and Catalytic Production of Sulfate Radicals in MOF-Derived CeO_2 center dot Co_3O_4 Nanoflowers for Efficient Degradation of Antibiotics, *Small*, 2021, **17**, 2102393.

32 Q. Wang, J. H. Lu, Y. Jiang, S. R. Yang, Y. Yang and Z. H. Wang, FeCo bimetallic metal organic framework nanosheets as peroxymonosulfate activator for selective oxidation of organic pollutants, *Chem. Eng. J.*, 2022, **443**, 136483.



33 L. L. Wang, X. Lan, W. Y. Peng and Z. H. Wang, Uncertainty and misinterpretation over identification, quantification and transformation of reactive species generated in catalytic oxidation processes: A review, *J. Hazard. Mater.*, 2021, **408**, 126998.

34 S. K. Han, T. M. Hwang, Y. Yoon and J. W. Kang, Evidence of singlet oxygen and hydroxyl radical formation in aqueous goethite suspension using spin-trapping electron paramagnetic resonance (EPR), *Chemosphere*, 2011, **84**, 1095–1101.

35 M. J. Xu, J. Li, Y. Yan, X. G. Zhao, J. F. Yan, Y. H. Zhang, B. Lai, X. Chen and L. P. Song, Catalytic degradation of sulfamethoxazole through peroxymonosulfate activated with expanded graphite loaded CoFe_2O_4 particles, *Chem. Eng. J.*, 2019, **369**, 403–413.

36 D. T. Oyekunle, J. Y. Cai, E. A. Gendy and Z. Q. Chen, Impact of chloride ions on activated persulfates based advanced oxidation process (AOPs): A mini review, *Chemosphere*, 2021, **280**, 130949.

37 L. S. Lian, B. Yao, S. D. Hou, J. Y. Fang, S. W. Yan and W. H. Song, Kinetic Study of Hydroxyl and Sulfate Radical-Mediated Oxidation of Pharmaceuticals in Wastewater Effluents, *Environ. Sci. Technol.*, 2017, **51**, 2954–2962.

38 Y. Zhou, J. Jiang, Y. Gao, J. Ma, S. Y. Pang, J. Li, X. T. Lu and L. P. Yuan, Activation of Peroxymonosulfate by Benzoquinone: A Novel Nonradical Oxidation Process, *Environ. Sci. Technol.*, 2015, **49**, 12941–12950.

39 Y. J. Feng, W. J. Sang, Z. Y. Deng, S. Y. Zhang and C. H. Li, Co-N-C@ SiO_2 core@shell architectures enhanced stability to activate peroxymonosulfate (PMS) for efficient sulfamethoxazole degradation, *Sep. Purif. Technol.*, 2022, **280**, 119783.

40 Z. J. Wang, Y. H. Li, G. H. Shen, Y. Q. Li, X. Y. Zhang, J. F. Gou and X. W. Cheng, Synthesis of CMK/LDH and CMK/CLDH for sulfamethoxazole degradation by PS activation: A comparative study of characterization and operating parameter, mechanism pathway, *Sep. Purif. Technol.*, 2021, **258**, 118018.

41 M. J. Xu, H. Y. Zhou, Z. L. Wu, N. W. Li, Z. K. Xiong, G. Yao and B. Lai, Efficient degradation of sulfamethoxazole by NiCo_2O_4 modified expanded graphite activated peroxymonosulfate: Characterization, mechanism and degradation intermediates, *J. Hazard. Mater.*, 2020, **399**, 123103.

42 L. L. Zhang, Y. L. Nie, C. Hu and J. H. Qu, Enhanced Fenton degradation of Rhodamine B over nanoscaled Cu-doped LaTiO_3 perovskite, *Appl. Catal., B*, 2012, **125**, 418–424.

43 I. Pokhrel, G. D. Reddy, T. Kwon, E. Choi, Y. S. Chun, S. T. Lee, B. J. Sung, D. H. Lee, H. B. Oh and K. B. Yoon, Insights into the directions to increase turnover frequency and turnover number during photochemical water oxidation with molecular Ru catalysts, *Energy Environ. Sci.*, 2022, **15**, 4259–4288.

